

Investigation of induced fission of ^{nat}Pb by accelerated ^7Li ions

N. A. Demekhina¹, G. S. Karapetyan², and V. Guimarães²

¹ Yerevan Physics Institute, Alikhanyan Brothers 2, Yerevan 0036, Armenia
Joint Institute for Nuclear Research (JINR), Flerov Laboratory of Nuclear Reactions (LNR), Joliot-Curie 6, Dubna 141980, Moscow region Russia

² Instituto de Física, Universidade de São Paulo, P. O. Box 66318, 05389-970 São Paulo, SP, Brazil

the date of receipt and acceptance should be inserted later

Abstract. Cross-sections for fragments produced by the fission reaction induced by accelerated ^7Li ions impinging into an ^{nat}Pb target at 245 MeV were obtained. We have applied the induced-activation method in off-line analysis. The analysis of charge and mass distributions of fission products allowed the determination of the total fission cross-section for the $^7\text{Li}+\text{Pb}$ system. The recoil technique (“thick target- thick catcher”), based on the two step model mathematical formalism, is used to determine the kinematics characteristics of reaction products. Analysis concerning transferred linear momentum provided information on the initial projectile-target interaction, and is compared with proton-induced fission measurements.

PACS. 2 5.85.Ge – 2 4.75.+i – 2 5.85.-w

1 Introduction

The investigation of nucleon-nucleus and nucleus-nucleus collision mechanisms at low and intermediate energies is a source of understanding the interplay between macroscopic and microscopic aspects of interaction in hot, high-spin nuclear matter. In this sense, fission mechanism of heavy nuclei has been the subject of investigation for many years. The way how collective nature of the nuclear fission is modified, according to the incident projectile type, the transferred energy, and the momentum as well, is a question of interest to both experimentalists and theorists. A considerable amount of measurements have been performed for nucleon-induced fission on different heavy nuclei [1]. Notwithstanding, a survey on the literature has displayed a considerable lack of experimental data for heavy-ion induced fission. There are some works on fission induced by carbon [2,3] and α -particles [4] projectiles. For lithium projectiles, a comprehensive investigation on fission of ^{208}Pb nucleus induced by ^6Li -ion beam, in the energy range of 74.8-94.4 MeV, has been performed by Vigdor *et al.* [5], where they quantitatively studied the decay properties of heavy nuclei, at high angular momentum and high excitation energy. It is of particular interest to investigate the dependence of the fission cross-section with the angular momentum transferred in the entrance channel when the fission is induced by nucleon- or heavy-ion projectiles. According to the classical rotating-liquid-drop model (RLDM) [6] and various other theoretical presentations [7,8,9,10], the fission barrier height should decrease monotonically, and eventually vanishes, as the transferred angular momentum increases. Furthermore, investigation

on fragments production due to fission induced by accelerated heavy ion can be of interest as possible application for the production of radioactive beams. High-energy fission induced by heavy nuclei could also be of interest for stimulated accelerator-driven systems (ADS's) for transmutation of nuclear waste, energy production, or other purposes where it is important to have knowledge of such nuclear reactions.

In this paper we present new results of a re-analysis of the data on fission reaction of lead target induced by ^7Li ion beam at 245 MeV. The previous analysis was presented in ref. [11] with some incorrect cross-sections due to the misuse of fission fragment registration efficiency. The cross sections for fission fragments between mass $60 < A < 150$ were then re-evaluated using charge and mass distributions and are present here in table 1. This mass region is assumed to have most of the fission fragments from binary fission since, for heavy nuclei, the fission is characterized by a broad mass distribution and it is the most probable decay channel in the energy range considered here. The new detection efficiencies considered in the present paper allowed us to calculate cross-section for 9 new fission fragments in the mass range of $A=61-69$ a.m.u. They are ^{61}Cu , ^{62}Zn , ^{65}Ni , ^{65}Zn , ^{65}Ga , ^{66}Ni , ^{66}Ga , ^{67}Ga and ^{69}Ge . Cross sections for some elements, ^{69m}Zn , ^{77}Kr , ^{85m}Y , ^{87}Kr , $^{87(m+g)}\text{Zr}$, ^{89m}Nb , ^{92m}Nb , ^{95m}Tc , ^{95}Ru , ^{96}Nb , ^{101}Pd , ^{105}Ru , $^{105(m+g)}\text{Ag}$, ^{105}Cd , ^{111m}Pd , ^{111}In , ^{111}Sn , ^{117g}In , ^{121}Xe , $^{126(m+g)}\text{Sb}$, ^{127g}Sn , ^{127}Cs , ^{133}La , ^{136}Cs , ^{137m}Ce , ^{141}Ce , ^{147}Eu , ^{148g}Pm , ^{148m}Pm and ^{148}Eu , presented in the previous paper were estimated to be just up to upper limits of their production this time, i.e., their photopeak yields were comparable to the background and

they were dropped out from the present analysis. Moreover, cross-sections for 29 elements present in the previous and present analysis, ^{67}Cu , ^{71m}Zn , ^{72}Zn , ^{72}Ga , ^{73}Ga , ^{75}Se , ^{75}Br , ^{76}As , $^{77(m+g)}\text{Br}$, ^{78}Ge , ^{78}As , ^{83}Rb , ^{84}Br , $^{84(m+g)}\text{Rb}$, ^{85g}Sr , ^{87m}Y , ^{89}Rb , ^{92}Sr , ^{92}Y , ^{94}Y , ^{95}Zr , $^{95(m+g)}\text{Nb}$, ^{95g}Tc , $^{96(m+g)}\text{Tc}$, ^{97}Zr , ^{121}I , $^{124(m+g)}\text{Sb}$, ^{133m}Ba , ^{140}Ba , were re-calculated. Some of the cross-sections were changed by the factor 6-7, some by 3-4. Cross-sections for some light nuclides fragments were also presented in the previous publication but their re-analysis will be considered in a further paper. Moreover, based on the dynamic model [8], it was possible to extract the angular momentum imparted to the fissioning nucleus at the interaction initial stage. The results were compared to the fission data of other systems also induced by heavy nuclei. In section-2 we describe the experimental procedure. In section-3 we present data analysis and the results on cross sections, while in section-4 we give some details on kinematic analysis of the reaction. Section-5 is devoted to the conclusion.

2 Experimental Procedure

The data here analysed was obtained by a measurement carried out by bombarding a natural lead target with an accelerated ^7Li -ion beam of energy 35 MeV/u from the U-400M cyclotron in the Joint Institute for Nuclear Research (JINR), Dubna, Russia. The target is composed of an assembling of seven foils, all together, of pure lead, having a natural isotopic composition (^{nat}Pb : 1.48% ^{204}Pb , 23.6% ^{206}Pb , 22.6% ^{207}Pb , and 52.3% ^{208}Pb), and a total thickness of 12 μm . The irradiation time was 40 min at ion beam intensity of about 10^{10} nuclei per second. Two aluminum foils, 20 μm thick each, located at forward and backward directions relative to the beam, providing a solid angle of about 2π , were used to collect the recoiled fragments from the fission on both sides of the target. The thickness of the catcher Aluminum foil was chosen to be larger than the longest recoil range of the fragments. The activity of the fission fragments were analysed in off-line mode by using the induced-activation method. The ranges and ratio of the emitted radioactive reaction products at forward and backward directions were also recorded. The spectra for the γ -rays emitted in the decays of radioactive fission products were measured from 10 min after the completion of the irradiation and lasted five months. HpGe detector with energy resolution of 0.23% at 1332 keV was used. The energy-dependent detection efficiency of the HpGe detector was measured with standard calibration sources of ^{22}Na , ^{54}Mn , $^{57;60}\text{Co}$, ^{137}Cs , ^{154}Eu , ^{152}Eu , and ^{133}Ba . The half-lives of identified isotopes were within the range between 15min and 1yr.

The error in determining cross sections for each fission fragments depended on the following factors: the statistical significance of experimental results ($\leq 2\text{-}3\%$), the accuracy in measuring the target thickness and the accuracy of tabular data on nuclear constants ($\leq 3\%$), and the errors in determining the energy dependence of the detector efficiency ($\leq 10\%$). Moreover, nuclear properties, such as

nuclear transition energies, intensities, and half-lives, used to identify the observed isotopes, were taken from ref. [12].

The reaction fragment production cross-sections, in the absence of a parent isotope, that may give a contribution in measured cross-section via β^\pm -decays, are usually considered as an independent yield (I) and it is determined by the following equation:

$$\sigma = \frac{\Delta N \lambda}{N_b N_n k \epsilon \eta (1 - \exp(-\lambda t_1)) \exp(-\lambda t_2) (1 - \exp(-\lambda t_3))} \quad (1)$$

where σ is the cross-section of the reaction fragment production (mb); ΔN is the yield of the photo-peak; N_b is the number of particles in the beam (min^{-1}); N_n is the number of target nuclei ($1/\text{cm}^2$); t_1 is the irradiation time; t_2 is the time of exposure between the end of the irradiation and the beginning of the measurement; t_3 is the time measurement; λ is the decay constant (min^{-1}); η is the intensity of γ -transitions; k is the total coefficient of γ -ray absorption in target and detector materials, and ϵ is the γ -ray-detection efficiency.

In the case where the yield of a given isotope includes a contribution from the β^\pm -decay of neighboring unstable isobars, the cross section calculation becomes more complicated [13]. If the formation probability for the parent isotope is known from experimental data, or if it can be estimated on the basis of other sources, hence the independent yields of daughter nuclei can be calculated by the relation:

$$\sigma_B = \frac{\lambda_B}{(1 - \exp(-\lambda_B t_1)) \exp(-\lambda_B t_2) (1 - \exp(-\lambda_B t_3))} \times \left[\frac{(\Delta N)_{AB}}{N_\gamma N_n k \epsilon \eta} - \sigma_A f_{AB} \frac{\lambda_A \lambda_B}{\lambda_B - \lambda_A} \left(\frac{(1 - \exp(-\lambda_A t_1)) \exp(-\lambda_A t_2) (1 - \exp(-\lambda_A t_3))}{(1 - \exp(-\lambda_B t_1)) \exp(-\lambda_B t_2) (1 - \exp(-\lambda_B t_3))} \right) \right]$$

where the subscripts A and B label variables refer to parent and daughter nucleus, respectively; the coefficient f_{AB} specifies the fraction of A nuclei decaying to a B nucleus ($f_{AB} = 1$, when the contribution from the β -decay corresponds 100%); and $(\Delta N)_{AB}$ is the total photo-peak yield associated with the decays of the daughter and parent isotopes. The effect of the precursor can be negligible in some limiting cases: where the half-life of the parent nucleus is very long, or in the case where its contribution is very small. In the case when parent and daughter isotopes could not be experimentally separated, the calculated cross-sections are classified as cumulative (C). It should be mentioned that the induced-activity method used here imposes some restrictions on the registration of the reaction products. The most severe of them is that it is not possible to measure stable and short-lived isotopes. We overcome this limitation by considering the charge and mass distribution analysis as explained in the following section.

3 Experimental Data Analysis

The experimental cross-sections of fission fragment production in the mass range of $60 \leq A \leq 150$ amu are presented in table 1 and fig. 1. The experimental points in the figure are the cross sections for each isobar chain of the observed fragments obtained by the induced-activity method. The solid black line is fission cross section for each mass number of fission products. To obtain this fission mass distribution, it is necessary to estimate the cross-sections for the isotopes not measurable by the induced-activity method. In the present work, therefore, we obtain these cross-sections by analysing the charge and mass distributions.

The charge distribution is assumed to have the following Gaussian function [13]:

$$\sigma_{A,Z} = \frac{\sigma_A}{(C\pi)^{1/2}} \exp\left(-\frac{(Z - Z_p)^2}{C}\right), \quad (3)$$

where $\sigma_{A,Z}$ is the independent cross-section for a given nuclide production with atomic charge Z and a mass number A ; σ_A is the isobaric cross-section of the mass chain A , Z_p denotes the most probable charge for a given isobar, and C denotes the width parameter of the charge distribution.

This kind of analysis for charge distribution has been reported earlier for fission experiments induced by different projectile at low energies on heavy targets [14, 15, 16]. What was observed in these works is that the charge distribution widths are practically independent on the excitation energy, projectile and target nuclear properties. Therefore, we assumed that the width parameter of the Gaussian is constant for different mass chains ($C = 1$). By fitting the distributions, using least-squares method, we obtained the most probable charge Z_p and σ_A parameters for a given isobar chain. At first, only independent (I) yields are used. Hence, during successive approximation procedures, the estimation of the independent component of cumulative cross-section is extracted. In table 2 we listed the most probable charges (Z_p) evaluated and their corresponding cross-sections. The values obtained here are in good agreement with data obtained for the fission of Bi target induced by ^{12}C projectile [15].

Figures 2-4 shows the calculated fractional cross-sections (cross-section of fragment production to total cross-section for given mass number), as well as their Gaussian charge distribution, for different isobaric chains, as a function of the difference ($Z_p - Z$). It can be proposed that charge distributions of fission fragments are mainly determined by the properties of forming nuclei.

To obtain the total fission cross section we analysed the mass distribution of fission fragments as a function of A . This mass distribution is assumed to be symmetric and given by a Gaussian function defined as [17]:

$$\sigma_f = \lambda_A \exp\left(-\frac{(A - M_A)^2}{\Gamma_A^2}\right), \quad (4)$$

the parameters λ_A , M_A and Γ_A stand for the height, mean mass M_A and width, respectively. The result of the sum

over all mass numbers of the fission fragments allows the estimation of the total fission cross-section. To avoid double counting due to the two fission fragments in each event, the sum of all cross-sections, was multiplied by a factor 0.5. The mass yield distribution obtained by the present fitting procedure is shown in fig. 1 (solid black curve). The values of the fit parameters, together with the obtained fission cross-section, are tabulated in table 3. The present mass distribution shows a maximum around mass $A = 103$. Therefore a mass $A = 206$ is expected for the fissioning nucleus in contrast with mass $A = 215$ of the compound nucleus. This indicates that about 9 nucleons (presumably neutrons), in average, were emitted during the fission process. This is reasonable, since a compound nuclear reaction of a charged particle and a heavy nucleus leads to an excitation energy well above the fission threshold (top of fission barrier).

4 Kinematics analysis

The kinematic analysis of the measured recoil nuclei were also performed in the frame of the two step vector model [18], described in detail in [11]. The kinetic energy T associated to each fragment can be determined from the recoil range values in the target, and with the help of the Northcliffe-Schilling tables [19]. To transform the ranges into kinetic energy of fission fragments we used the relation:

$$R = KT^{N/2}, \quad (5)$$

where the parameters K and N are obtained, for a given Z and A , by fitting the range dependence on energy of accelerated ions. By its turn, to obtain the recoil range in the target material, $R = 2W(F + B)$, as well as the forward-backward (F/B) ratio of product emission, where here W is the thickness of the target in mg/cm^2 , we have taken the relative amount of radioactive products in the forward (F) and backward (B) at the catcher foils. These amounts are given by:

$$F = \frac{S_F}{S_F + S_B + S_T}, \quad B = \frac{S_B}{S_F + S_B + S_T}, \quad (6)$$

where S_F , S_B , and S_T are the photo-peak yields associated with the radioactive products from the catcher foils (forward and backward) and in the target.

Also, from the kinetic energy, we can estimate the mean excitation energy and consequently the corresponding relative parallel momentum of each pair of fragments, p_{\parallel}/p_{CN} , where p_{CN} is the momentum of a hypothetical compound nucleus formed in a complete fusion. They are related by the following expression [20]:

$$\frac{E^*}{E_{CN}} = 0.8 \frac{p_{\parallel}}{p_{CN}} \quad (7)$$

These kinematic parameters for some fragments obtained in present work are given in table 4. The total kinetic energy released in each fission process can be determined as a sum of the energies of two presumed fragments. For the present fission process the total kinetic energy is estimated to be 141 ± 13 MeV, on average, which is in fairly good agreement with 142.7 MeV estimated from the statistical approximation [21].

The energy regime of fission reaction induced by heavy particles is an important parameter to discuss the mechanism of the process. Reactions where incident particle velocity is higher than Fermi velocity of the nucleons in the compound nucleus, the individual nucleon-nucleon interaction dominates over the nucleus-nucleus interaction in the entrance channel, affecting the statistical description of the reaction. Saint Laurent *et al* [22] proposed that an important kinematic parameter to describe the change of the energy regime is the linear momentum imparted to the target nucleus. They have plotted the average parallel momentum transferred as a function of the projectile incident energy, both quantity divided by the mass number of the projectile, for available data on fission reactions induced by protons, alphas, deuterium on Thorium and Uranium as well as heavy incident particles such as ^{16}O and ^{20}Ne on Uranium, and compared with the full momentum transferred, see their fig. 2 in ref. [22]. Full momentum transferred would correspond to the momentum for the compound nucleus formation and smaller transferred momentum may indicate the system lacks of complete fusion process. The authors in ref. [22] have then proposed that the energy regime for fission induced by heavy particles could be divided in three energy regions: (i) low-energy range, $E/A \leq 10$ MeV/u and $p_{\parallel}/p_{CN} \sim 1$, where complete fusion is the dominate process; (ii) intermediate energy range, $10 \text{ MeV/u} \leq E/A \leq 70 \text{ MeV/u}$, where p_{\parallel}/p_{CN} decreases progressively down to 0.5, i.e., about half of the incident beam momentum is transferred to the target. At such energies, there is an indication that transferred momentum is proportional to the mass of the projectile; (iii) high energy range, $70 \text{ MeV/u} \leq E \leq 1000 \text{ MeV/u}$, where there is a drastic decrease of the momentum transferred to the target as compared with full momentum transferred.

In our case, for $E/A = 35 \text{ (MeV/u)}$, we are in the regime region ii). The average value of the linear momentum transferred divided by full momentum transferred to the target obtained in the present study is $p_{\parallel}/p_{CN} = 0.46 \pm 0.09$. Our data support the suggestion that for the energy regime between 10 MeV/u and 70 MeV/u, the p_{\parallel}/p_{CN} decreases down to 0.5, but remains approximately independent of the target mass and of the projectile identity. Thus, our data can confirm that a complete fusion is not the dominant process at the energy regarded. In this intermediate energy region, the complete fusion process at low limits are replaced partially by other processes, as the energy increases. We can say that only approximately 40% of the fission channel at this energy can result from complete fusion. The remain momentum transferred could be connected to incomplete fusion, or a significant pre-

equilibrium contribution of the emission of nucleons or light nuclei.

The mean excitation energies for the present reaction was estimated to be $E^* = 90 \pm 18$ MeV, correspond to nuclear temperature $T = 1.9 \pm 0.2$ MeV. Excitation energy and temperature are related by the expression $aT^2 + 4T = E^*$ [23], where $a = A/8$ is the level-density parameter and A is the mass of the compound nucleus. Our value for the mean excitation energy is similar to the one obtained for the fission reaction of $^6\text{Li} + ^{208}\text{Pb}$ system at 94.4 MeV [5], $E^* = 100$ MeV ($T = 2.1$ MeV). We can conclude that, in our case, where the incident energy for ^7Li beam is higher, the contribution of the fusion process is much reduced as the proposition asserted by authors in [22].

The fission cross-section in the present work was found to be 605 ± 91 mb. The ratio between the fission cross-section σ_f and the fission cross-section for the proton-induced fission at the same excitation energy [1] is a factor 5 times higher. Such fission cross-section increment can be associated with a higher angular momentum transferred by the accelerated heavier ion during the fission process. This can be related to a higher rotation energy impinged by heavier projectile to the compound nucleus. As it is well known from different macroscopic and microscopic models [6, 7, 8, 9, 10], the rotational energy of hot nuclei strongly affects the fission probability. According to the dynamic model [8], the initial relative kinetic energy and angular momentum of the projectile, in a heavy-ion induced fission reaction, is converted into the intrinsic excitation energy and the spin of the fused compound system. The equilibrium is determined by the balance of the macroscopic surface energy, Coulomb energy, and the rotational energy. The concept of dynamical force equilibrium in the entrance reaction channel serves as a criteria to the determination of the average and maximum angular momentum transferred for different colliding systems. According to the model, transferred linear momentum should be a decreasing function of the impact parameter b . Furthermore, the value of a maximum angular momentum ℓ_{max} corresponds to a peripheral collision is defined by:

$$\ell_{max} = R \sqrt{\frac{2\mu(E_{c.m.} - V_{CB})}{\hbar^2}}. \quad (8)$$

Here, R is the maximum distance between two nuclei at which the collision leads to a reaction, μ is the reduced mass and V_{CB} is the Coulomb energy of the system at distance R ; $E_{c.m.}$ is at the center-of-mass bombarding energy.

For the present study for the $^7\text{Li} + \text{Pb}$ system at $E_{c.m.} = 237$ MeV, the maximum angular momentum is $\ell_{max} \sim 90 \hbar$. The average angular momentum imparted into the fissile system at energies above the barrier can also be derived using the following equation [9]:

$$\langle \ell \rangle = \frac{2}{3} \sqrt{\frac{2\mu R^2 (E_{c.m.} - V_{CB})}{\hbar^2}}. \quad (9)$$

In our case, the average angular momentum is estimated to be about $\langle \ell \rangle = 55\text{-}60 \hbar$. The interval is because the spin distribution is not a sharp cutoff. For comparison, the value of the average angular momentum obtained for the $^6\text{Li}+^{208}\text{Pb}$ system at 94.4 MeV, corresponding to a complete fusion cross section, is 30-35 \hbar . Also, for a higher incident energy of the projectile, as our case, the number of evaporated neutrons should increase, opening new fission channels. As a result, not only the fission cross section should be higher but we also observed a broad distribution of transferred linear momentum and excitation energy, as shown in table 4. For $^6\text{Li}+^{208}\text{Pb}$ system at 94.4 MeV the average angular momentum is lower, and therefore it seems that the entire linear momentum is transferred to the compound nucleus. The variety of fragments in the present work with high and low linear momentum is also an indication of possible incomplete-fusion mechanism, as expected for a system in such range of energy.

As known, the presence of angular momentum lowers the fission-barrier heights [6,7,8,9,10] and it can be used to analyze the energy dependence of the excited nucleus fissionability [24]. In our case, fission is expected to play a significant role for angular momentum above 50 \hbar , when the fission barrier has dropped to about half of the previous value, at zero angular momentum. The fission-barrier dependence on the angular momentum can be neglected in the case of nucleon-nucleus interaction at intermediate energies, where only a small angular momentum is imparted to the compound nucleus by the incident nucleon. On the another hand, it becomes relevant for higher values for ℓ , in heavy-ion-induced reactions. It provides a careful and cogent explanation for the higher fission cross-section in the present investigation as compared with fission induced by protons or neutrons.

5 Conclusion

New analysis of the data regarding the fission process of $^7\text{Li}+^{nat}\text{Pb}$ at intermediate energies 245 MeV is presented. The fission cross-section, derived from the analysis of the obtained charge and mass distributions was equal to 605 ± 91 mb. This value exceeds the cross section obtained for fission induced by protons at approximately the same energy range. This can be explained by the effect of the transferred angular momentum, which is much higher for heavy ion-induced reaction.

The measurement of the recoil fission fragments, and by considering their kinematic properties, in the frames of two step models, allowed the calculation of some important reaction parameters such as relative transferred momentum. The average relative value of the transferred momentum p_{\parallel}/p_{CN} (where p_{CN} is the total momentum of the hypothetical complete nucleus), obtained in the present analysis is 0.46 ± 0.09 . This value contain the information on the initial reaction mechanism, and indicates that, in the energy regime investigated, the fission process does not proceed solely via the compound nucleus formation. Other mechanisms may take participation on the first step

reaction, and only 40% of all fission events are resultant of compound nucleus fission.

Regarding the dynamic model-based calculation, the fissile system is assumed to be formed at an intermediate energy with high angular momentum. This might be the explanation for the high value of fission cross-section for heavy-ion-induced fission.

G. Karapetyan would like to thank Fundação de Amparo à Pesquisa do Estado de São Paulo (FAPESP) 2011/00314-0 for the financial support and International Centre for Theoretical Physics (ICTP) under the Associate Grant Scheme.

References

1. A. V. Prokofiev, Nucl.Instrum. Methods A **463**, 557 (2001).
2. A. Mukherjee, D. J. Hinde, M. Dasgupta, *et al.*, Phys. Rev. C **75**, 044608 (2007).
3. R. N. Sagaidak, G. N. Kniajeva, I. M. Itkis, *et al.*, Phys. Rev. C **68**, 014603 (2003).
4. A. Ingemarsson, J. Nyberg, P. U. Renberg, *et al.*, Nucl. Phys. A **676**, 3 (2000).
5. S. E. Vigdor, H. J. Karwowski, W. W. Jacobs, *et al.*, Phys. Rev. C **26**, 1035 (1982).
6. S. Cohen, F. Plasil, and W. J. Swiatecki, Ann. Phys. (N. Y.) **82**, 557 (1974).
7. A. J. Sierk, *et al.*, Phys. Rev. C **33**, 2039 (1986).
8. J. Wilczynski, Nucl. Phys. A **216**, 386 (1973).
9. O. A. Capurro, D. E. DiGregorio, S. Gil, *et al.*, Phys. Rev. C **55**, 766 (1997).
10. M. G. Mustafa, K. Kumar, Phys. Rev. C **12**, 1638 (1975).
11. N. A. Demekhina, G. S. Karapetyan, S. M. Lukyanov, *et al.*, Phys. At. Nucl. **68**, 21 (2005).
12. R. B. Firestone, in Tables of Isotopes, 8th ed.: 1998 Update (with CD ROM), edited by S. Y. Frank Chu (CD-ROM editor) and C. M. Baglin (Wiley Interscience, New York, 1996).
13. H. Baba, J. Sanada, H. Araki, *et al.*, Nucl. Instr. Methods A **416**, 301 (1998).
14. H. Kudo, M. Maruyama, and M. Tanikawa, *et al.*, Phys. Rev. C **57**, 178 (1998).
15. C. L. Branquinho and V. J. Robinson, J. Inorg. Nucl. Chem. **39**, 921 (1977).
16. A. C. Wahl, R. L. Ferguson, *et al.*, Phys. Rev. **126**, 776 (1962).
17. M.C. Duijvestijn, A.J. Koning, *et al.*, Phys. Rev. C **59**, 776 (1999).
18. L. Winsberg, Phys. Rev. C **22**, 2116(1980) .
19. L. C. Northcliffe and R. E. Schilling, Nucl. Data, Sect. A **7**, 233 (1970).
20. M. Lagarde-Simonoff and G. M. Simonoff, Phys. Rev. C **20**, 1498 (1979).
21. V. E. Viola, K. Kwiatkowski, and M. Walker, Phys. Rev. C **31**, 1550 (1985).
22. F. Saint-Laurent, M. Conjeaud, R. Dayrasv, *et al.*, Phys. Lett. B **110**, 372 (1982).
23. J. M. Blatt and V. F. Weisskopf, Theoretical Nuclear Physics (Wiley, New York, 1952).
24. S. G. Mashnik, Acta Phys. Slov. **43**, 243 (1993).

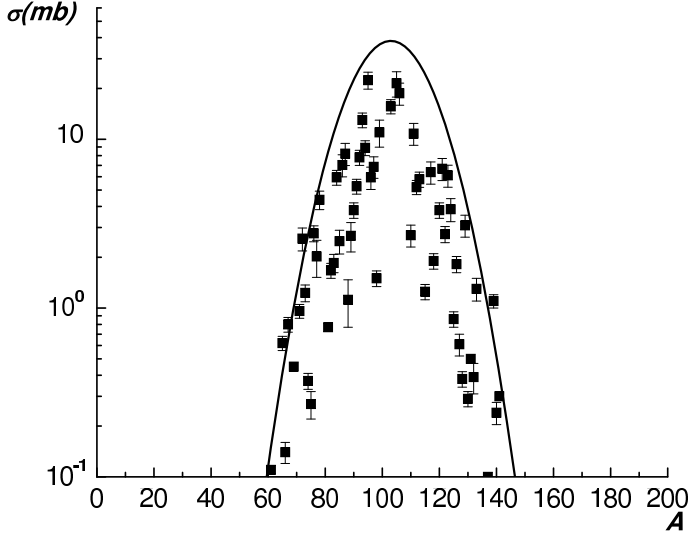


Fig. 1. Experimental cross sections for the fission-products mass distribution of 245 MeV ^7Li -induced fission on ^{nat}Pb . The black continuous curve corresponds to the derived fission cross-section as a function of the mass of the fragments after taking into account the estimation of the no-detected isotopes.

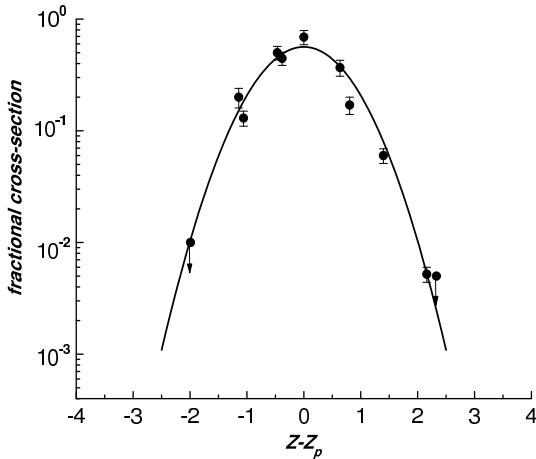


Fig. 2. The charge distribution of fission products for the 245 MeV ^7Li -induced fission on ^{nat}Pb for isobaric chains in the mass region $A=72-78$. The curves are the estimated Gaussian distributions.

Table 1. Cross-sections of fission fragments. *C* and *I* stands for independent and cumulative cross sections as explained in the text.

Element	Type	σ , mb	Element	Type	σ , mb
^{61}Cu	C	<0.11	^{99}Mo	C	10.7 ± 1.1
^{62}Zn	C	<0.04	^{99m}Tc	I	0.26 ± 0.03
^{65}Ni	I	≤ 0.20	^{101m}Rh	I	0.78 ± 0.08
^{65}Zn	I	0.40 ± 0.08	^{102m}Rh	I	0.42 ± 0.03
^{65}Ga	C	≤ 0.02	^{103}Ru	C	15.7 ± 1.5
^{66}Ni	I	0.11 ± 0.02	$^{105(m+g)}\text{Rh}$	I	13.7 ± 1.4
^{66}Ga	I	≤ 0.035	^{106}Ru	C	11.1 ± 1.1
^{67}Cu	C	0.72 ± 0.07	^{106m}Rh	C	7.60 ± 0.91
^{67}Ga	C	0.026 ± 0.003	^{110m}Ag	I	2.70 ± 0.40
^{69}Ge	C	≤ 0.45	$^{111(m+g)}\text{Ag}$	C	10.2 ± 1.0
^{71m}Zn	I	0.96 ± 0.14	^{111}Cd	I	≤ 0.63
^{72}Zn	I	≤ 0.02	^{112}Pd	C	3.10 ± 0.31
^{72}Ga	I	0.25 ± 0.02	^{112}Ag	I	2.10 ± 0.25
^{73}Ga	I	0.63 ± 0.08	$^{113(m+g)}\text{Ag}$	C	2.45 ± 0.37
^{74}As	I	0.37 ± 0.04	$^{113(m+g)}\text{Sn}$	C	3.34 ± 0.50
^{75}Se	I	0.19 ± 0.01	^{115}Cd	C	1.25 ± 0.13
^{75}Br	C	≤ 0.017	^{117g}Cd	C	1.26 ± 0.13
^{76}As	I	2.77 ± 0.28	^{117m}Cd	C	1.31 ± 0.16
$^{77(m+g)}\text{Ge}$	C	2.00 ± 0.20	^{117m}Sn	I	2.83 ± 0.28
$^{77(m+g)}\text{Br}$	I	≤ 0.02	$^{118(m+g)}\text{Sb}$	I	1.90 ± 0.20
^{78}Ge	I	2.40 ± 0.24	^{120m}Sb	I	3.80 ± 0.40
^{78}As	C	<1.98	^{121g}Te	I	4.60 ± 0.69
^{81m}Se	C	≤ 0.77	^{121m}Te	I	1.95 ± 0.29
$^{82(m+g)}\text{Br}$	I	1.67 ± 0.17	^{121}I	I	≤ 0.45
^{83}Rb	C	1.85 ± 0.19	$^{122(m+g)}\text{Sb}$	I	2.74 ± 0.30
^{84}Br	C	4.80 ± 0.50	^{123m}Te	I	4.73 ± 0.50
$^{84(m+g)}\text{Rb}$	I	1.14 ± 0.11	^{123}I	I	0.94 ± 0.10
^{85g}Sr	I	1.80 ± 0.18	^{123}Xe	C	≤ 0.04
^{85m}Sr	I	≤ 0.34	$^{124(m+g)}\text{Sb}$	I	2.60 ± 0.26
^{85g}Y	C	0.35 ± 0.04	^{124}I	I	1.25 ± 0.13
$^{86(m+g)}\text{Rb}$	I	7.0 ± 1.1	^{125}Sb	C	0.86 ± 0.09
^{87g}Y	I	0.68 ± 0.07	^{126}I	I	1.82 ± 0.19
^{87m}Y	C	0.50 ± 0.06	^{127}Sb	C	≤ 0.06
^{88}Y	C	1.12 ± 0.35	$^{127(m+g)}\text{Xe}$	I	0.29 ± 0.03
^{89}Rb	C	2.20 ± 0.22	^{128}Sb	C	0.38 ± 0.04
$^{89(m+g)}\text{Zr}$	C	0.48 ± 0.05	^{129}Sb	C	≤ 0.55
^{90m}Y	I	3.80 ± 0.40	^{129m}Te	I	1.62 ± 0.17
^{91}Sr	C	4.94 ± 0.50	^{129g}Ba	C	≤ 0.73
^{91m}Y	I	≤ 0.32	^{129m}Ba	C	≤ 0.19
^{92}Sr	C	5.80 ± 0.58	$^{130(m+g)}\text{I}$	I	0.29 ± 0.03
^{92}Y	I	2.00 ± 0.20	^{131m}Te	C	≤ 0.50
^{93}Y	C	13.0 ± 1.3	^{132}Te	C	≤ 0.02
^{94}Y	C	8.90 ± 0.90	^{132}Cs	I	0.37 ± 0.04
^{95}Zr	C	12.0 ± 1.2	$^{133(m+g)}\text{I}$	C	≤ 1.00
$^{95(g+m)}\text{Nb}$	I	9.8 ± 1.0	^{133m}Ba	I	0.30 ± 0.06
^{95g}Tc	I	≤ 0.10	^{139}Ba	C	≤ 0.45
$^{96(g+m)}\text{Tc}$	I	≤ 0.03	$^{139(m+g)}\text{Ce}$	C	1.17 ± 0.12
^{97}Zr	C	3.12 ± 0.31	^{140}Ba	C	0.33 ± 0.03
$^{97(g+m)}\text{Nb}$	I	3.55 ± 0.36	^{140}La	I	0.18 ± 0.02
^{97}Ru	C	≤ 0.20	^{141}La	I	≤ 0.30
^{98m}Nb	I	1.50 ± 0.16	^{147}Gd	C	≤ 0.03

Table 2. Values of the most probable charge Z_p and their corresponding cross sections.

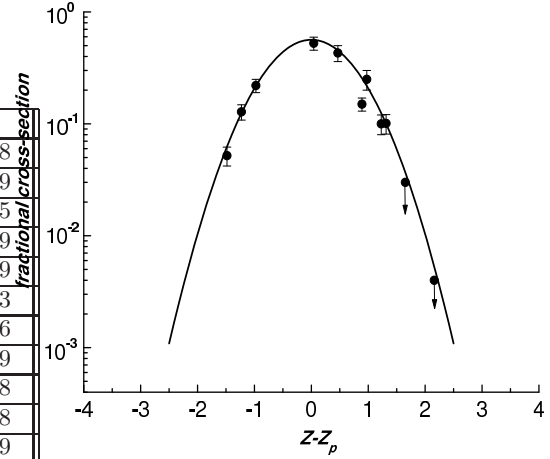
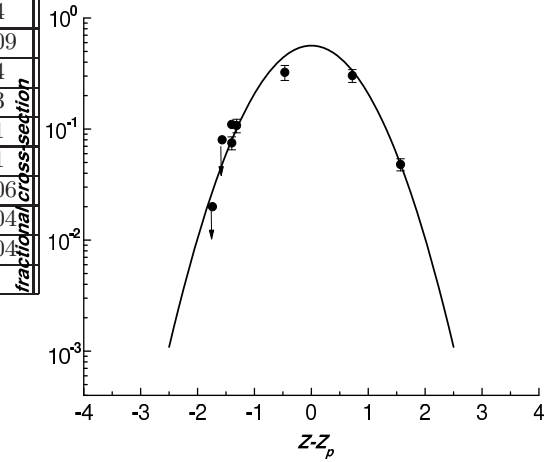
A	Z_p	σ_A	A	Z_p	σ_A
76	33.0 ± 0.7	4.0 ± 0.4	110	45.7 ± 0.7	30.0 ± 0.8
77	32.5 ± 0.5	4.0 ± 0.3	111	46.3 ± 0.6	30.0 ± 1.9
78	32.4 ± 0.3	5.4 ± 0.9	112	45.6 ± 0.5	27.0 ± 1.5
82	34.0 ± 0.2	9.6 ± 0.8	113	48.6 ± 0.5	32.0 ± 0.9
83	35.9 ± 0.2	11.0 ± 0.5	115	49.4 ± 0.7	24.0 ± 0.9
84	35.6 ± 0.3	12.0 ± 0.6	117	49.2 ± 0.6	20.0 ± 1.3
85	36.7 ± 0.5	14.0 ± 0.7	118	49.7 ± 0.5	18.8 ± 0.6
86	36.5 ± 0.5	15.5 ± 0.5	120	50.1 ± 0.3	15.0 ± 0.9
89	37.3 ± 0.5	21.0 ± 1.4	121	51.5 ± 0.6	15.0 ± 0.8
90	37.8 ± 0.5	24.0 ± 0.5	121	51.5 ± 0.5	15.0 ± 0.8
91	37.0 ± 0.3	24.0 ± 1.2	122	52.0 ± 0.3	12.0 ± 0.9
92	37.6 ± 0.4	28.0 ± 1.0	123	51.8 ± 0.4	9.0 ± 0.1
93	39.4 ± 0.4	27.0 ± 1.2	124	51.8 ± 0.5	9.0 ± 0.3
94	39.5 ± 0.5	30.0 ± 1.0	125	52.3 ± 0.4	8.0 ± 0.4
95	40.4 ± 0.3	25.0 ± 1.3	126	52.3 ± 0.3	6.00 ± 0.09
96	40.1 ± 0.2	23.0 ± 0.8	127	52.6 ± 0.4	6.0 ± 0.4
97	41.3 ± 0.6	30.0 ± 1.1	128	52.7 ± 0.5	4.5 ± 0.3
99	41.4 ± 0.4	34.0 ± 0.8	129	52.4 ± 0.3	5.0 ± 0.1
101	43.2 ± 0.3	38.0 ± 1.1	130	54.4 ± 0.3	3.9 ± 0.1
102	43.1 ± 0.5	37.0 ± 0.7	132	54.0 ± 0.4	2.00 ± 0.06
103	43.5 ± 0.4	38.0 ± 0.7	140	56.2 ± 0.2	0.60 ± 0.04
105	44.7 ± 0.5	30.0 ± 0.6	141	56.2 ± 0.5	0.40 ± 0.04
106	44.3 ± 0.4	30.0 ± 1.1			

Table 3. Values of the parameters obtained in the fitting procedure of the mass distribution and fission cross-section σ_f .

Γ_A	17.84 ± 0.89
λ_A	38.3 ± 2.3
M_A	103.0 ± 0.2
σ_f (mb)	605 ± 91

Table 4. Kinematic parameters of fission fragments.

Nucleus	F/B	$2W(F+B)$, mg/cm ²	T (MeV)	E^* (MeV)	p_{\parallel}/p_{CN}
^{72}Zn	1.11 ± 0.22	13.2 ± 2.6	107 ± 22	69 ± 12	0.33 ± 0.06
$^{77(m+g)}\text{Br}$	1.16 ± 0.14	13.4 ± 1.6	100 ± 12	82 ± 12	0.42 ± 0.06
$^{82(m+g)}\text{Br}$	1.17 ± 0.14	11.8 ± 1.4	96 ± 12	84 ± 12	0.43 ± 0.06
^{83}Rb	1.17 ± 0.08	10.25 ± 0.72	93 ± 7	80 ± 8	0.41 ± 0.04
$^{84(m+g)}\text{Rb}$	1.14 ± 0.10	8.17 ± 0.74	90 ± 8	69 ± 8	0.35 ± 0.04
$^{87(m+g)}\text{Y}$	1.19 ± 0.06	10.50 ± 0.53	88 ± 4	86 ± 4	0.44 ± 0.02
^{91}Sr	1.18 ± 0.10	10.10 ± 0.81	79 ± 6	76 ± 8	0.39 ± 0.04
^{95}Zr	1.19 ± 0.16	11.4 ± 1.7	77 ± 12	78 ± 12	0.40 ± 0.06
$^{95(g+m)}\text{Nb}$	1.23 ± 0.11	11.3 ± 1.0	77 ± 7	90 ± 8	0.46 ± 0.04
$^{96(g+m)}\text{Tc}$	1.29 ± 0.14	10.1 ± 1.1	75 ± 8	100 ± 10	0.58 ± 0.06
^{99}Mo	1.22 ± 0.06	10.33 ± 0.52	72 ± 4	84 ± 4	0.43 ± 0.02
$^{105(m+g)}\text{Rh}$	1.17 ± 0.09	10.07 ± 0.81	71 ± 6	67 ± 4	0.34 ± 0.02
$^{111(m+g)}\text{Ag}$	1.22 ± 0.12	8.32 ± 0.83	66 ± 7	76 ± 8	0.39 ± 0.04
^{115}Cd	1.19 ± 0.12	10.8 ± 1.1	59 ± 6	65 ± 8	0.33 ± 0.04
$^{117(m)}\text{Sn}$	1.43 ± 0.17	7.69 ± 0.92	54 ± 6	119 ± 16	0.61 ± 0.08
^{120m}Sb	1.45 ± 0.06	4.29 ± 0.17	51 ± 2	119 ± 8	0.61 ± 0.04
^{124}I	1.65 ± 0.18	7.95 ± 0.87	45 ± 5	150 ± 15	0.77 ± 0.08


Fig. 3. Idem for isobaric chains in the mass region $A=115-118$.

Fig. 4. Idem for isobaric chains in the mass region $A=125-130$.